JACS
JOURNAL OF THE AMERICAN CHEMICAL SOCIETY
pubs.acs.org/JACS
Article

Effect of Linker Distribution in the Photocatalytic Activity of Multivariate Mesoporous Crystals

Belén Lerma-Berlanga, Carolina R. Ganivet, Neyvis Almora-Barrios, Sergio Tatay, Yong Peng, Josep Albero, Oscar Fabelo, Javier González-Platas, Hermenegildo García, Natalia M. Padial,* and Carlos Martí-Gastaldo*

Cite This: J. Am. Chem. Soc. 2021, 143, 1798−1806

ABSTRACT: The use of Metal−Organic Frameworks as crystalline matrices for the synthesis of multiple component or multivariate solids by the combination of different linkers into a single material has emerged as a versatile route to tailor the properties of single-component phases or even access new functions. This approach is particularly relevant for Zr_6-MOFs due to the synthetic flexibility of this inorganic node. However, the majority of materials are isolated as polycrystalline solids, which are not ideal to decipher the spatial arrangement of parent and exchanged linkers for the formation of homogeneous structures or heterogeneous domains across the solid. Here we use high-throughput methodologies to optimize the synthesis of single crystals of UiO-68 and UiO-68-TZDC, a photoactive analogue based on a tetrazine dicarboxylic derivative. The analysis of the single linker phases reveals the necessity of combining both linkers to produce multivariate frameworks that combine efficient light sensitization, chemical stability, and porosity, all relevant to photocatalysis. We use solvent-assisted linker exchange reactions to produce a family of UiO-68-TZDC$_{\%}$ binary frameworks, which respect the integrity and morphology of the original crystals. Our results suggest that the concentration of TZDC in solution and the reaction time control the distribution of this linker in the sibling crystals for a uniform mixture or the formation of core−shell domains. We also demonstrate how the possibility of generating an asymmetric distribution of both linkers has a negligible effect on the electronic structure and optical band gap of the solids but controls their performance for drastic changes in the photocatalytic activity toward proton or methyl viologen reduction.

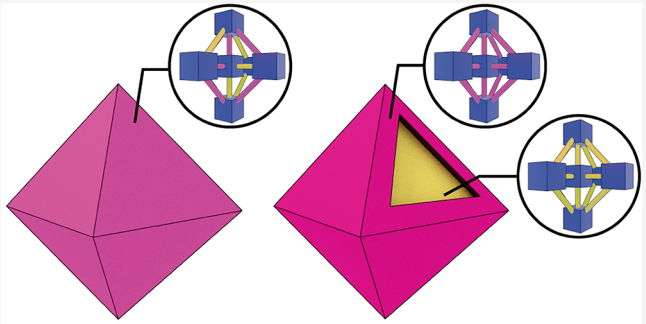

INTRODUCTION

The discovery of the family of Zr(IV) UiO-type Metal−Organic Frameworks (MOFs) by Lillerud and co-workers in 2008 introduced a versatile platform for the design of MOFs with excellent stability.[1] Since then, the use of monocarboxylic acids as modulators[2] combined with the flexibility of $[Zr_6O_4(OH)_4(CO_2)_{12}]$ clusters acting as inorganic nodes, has enabled us to gain chemical control over the design of isoreticular frameworks with linear dicarboxylic linkers for a huge family of porous materials with tailorable micro/mesoporosity and application in catalysis, gas storage, or separation technologies.[3,4] Unfortunately, most of these materials can be only synthesized as polycrystalline solids, highlighting the difficulties in isolating single crystals. This problem is even more severe for the mesoporous derivatives, which require the use of elongated linkers with very poor solubility in the organic solvents used in the synthesis. This is possibly why the synthesis of single crystals of UiO-68 using H_2TPDC ([1,1′:4′,1″-terphenyl]-4,4″-dicarboxylic acid) linkers still remains elusive, and all crystals available rely on amine, alcohol, or alkyl derivatives with subsequent changes to the porosity or physical properties of the pristine material.[5−7]

The availability of single crystals is particularly important in understanding the dynamic exchange reactions often used to produce multivariate frameworks by postsynthetic (PSE)[8] or solvent-assisted linker exchange (SALE).[9] The porosity of the framework and the concentration of the exchanged linker control the diffusion of the last. As a result, these variables can impose changes to the microstructure and distribution of exchanged and parent linkers in the framework. Both features might modify the physical properties and performance of the MOF in specific applications. This phenomenon was originally demonstrated for microporous MOF-5, UMCM-8, and UiO-66,[10] but there are no precedents for mesoporous frameworks.

Received: August 26, 2020
Published: January 12, 2021

https://dx.doi.org/10.1021/jacs.0c09015
J. Am. Chem. Soc. 2021, 143, 1798−1806

Built upon our recent experience for the challenging chemistry of titanium,[11−13] here we use High-Throughput (HT) synthetic methodologies[14] to optimize the conditions required for isolating single crystals of pristine UiO-68 and its photoactive analogue UiO-68-TZDC, based on 4,4′-(1,2,4,5-tetrazine-3,6-diyl)dibenzoic acid (H_2TZDC). The availability of crystals is used to analyze the effect of TZDC concentration in the formation of binary frameworks by SALE. Our results confirm that the crystals evolve from an ordered core−shell microstructure of TZDC/TPDC linkers into a more homogeneous distribution for increasing equivalents of the exchanged linker. By correlating the electronic structure of UiO-68-TZDC$_{\%}$ solids with their photocatalytic activity, we demonstrate the impact of linker distribution over the photocatalytic performance of multivariate mesoporous crystals.

RESULTS AND DISCUSSION

High-Throughput Synthesis of UiO-68 Single Crystals. We designed a first experiment for optimizing the formation of UiO-68 crystals that accounted for systematic variations of temperature (90, 100, or 120 °C), reaction time (48 or 72 h), and equivalents of acid modulator (trifluoroacetic acid (TFA), acetic acid (AcOH), benzoic acid (BA), or formic acid (FA)). The metal/linker stoichiometry, zirconium source, and solvent were fixed according to the protocols adopted by the community to 1:1, $ZrCl_4$ and *N*,*N*-dimethylformamide (DMF)[12] for a library of over 80 reactions. We used a FLEX SHAKE HT workstation from Chemspeed for robotic dispensing of solids and liquids combined with a 96-well Powder X-Ray Diffraction (PXRD) plate. This helped in maintaining a high reproducibility and accelerating the systematic screening of reaction parameters based on the crystallinity and PXRD fingerprints of the products. See Supporting Information, SI, Section S2 for more experimental details. As shown in the ternary diagrams in Figure S4, crystals of UiO-68 were only formed by reaction with 40 equiv of TFA at 100 °C over 72 h. The solid was isolated as pale-yellow crystals with octahedral morphology and sizes ranging from 20 to 50 μm (Figure 1a left). To challenge the versatility of these synthetic conditions we next synthesized H_2TZDC by replacing the central phenyl ring in H_2TPDC with an *s*-tetrazine ring. Tetrazine derivates are electroactive molecules capable of undergoing reversible transformation into stable anion radicals. As a result, their fluorescence can be electrochemically switched for applications in light generation, sensors, and polymers.[15,16] These features can also be translated to MOFs for generating photoactive frameworks by reticulation of tetrazine derivatives.[17] Despite the poorer solubility of the tetrazine linker, the conditions optimized for TPDC only required a slight reduction of the modulator equivalents, from 40 to 10, to isolate UiO-68-TZDC as pink octahedral crystals with sizes ranging from 10 to 20 μm (Figure 1a right). These conditions are substantially different to the reported synthesis of polycrystalline UiO-68-TZDC for particle sizes near 1 μm.[18]

UiO-68 and UiO-68-TZDC crystallize in the cubic space group *Fm*-3*m* (*a* = 32.71 and 32.47 Å, respectively). They display an expanded cubic closed-packed structure for the characteristic 12-connected *fcu* topology of the UiO family.[1] See SI Section S3 for more details. The impact of the linker replacement in the porosity metrics is almost negligible for octahedral and tetrahedral voids of 27.3 and 19.3 Å (Figure 1b,c). As for the internal structure of the linkers, the carboxylate groups remain coplanar in both cases but the central ring presents a certain degree of disorder. We collected crystallographic data at 100 K (UiO-68) and at room temperature (UiO-68-TZDC). The disorder is present in both cases which suggests this is intrinsic to the crystallographic packing of the solids and not thermal in origin.

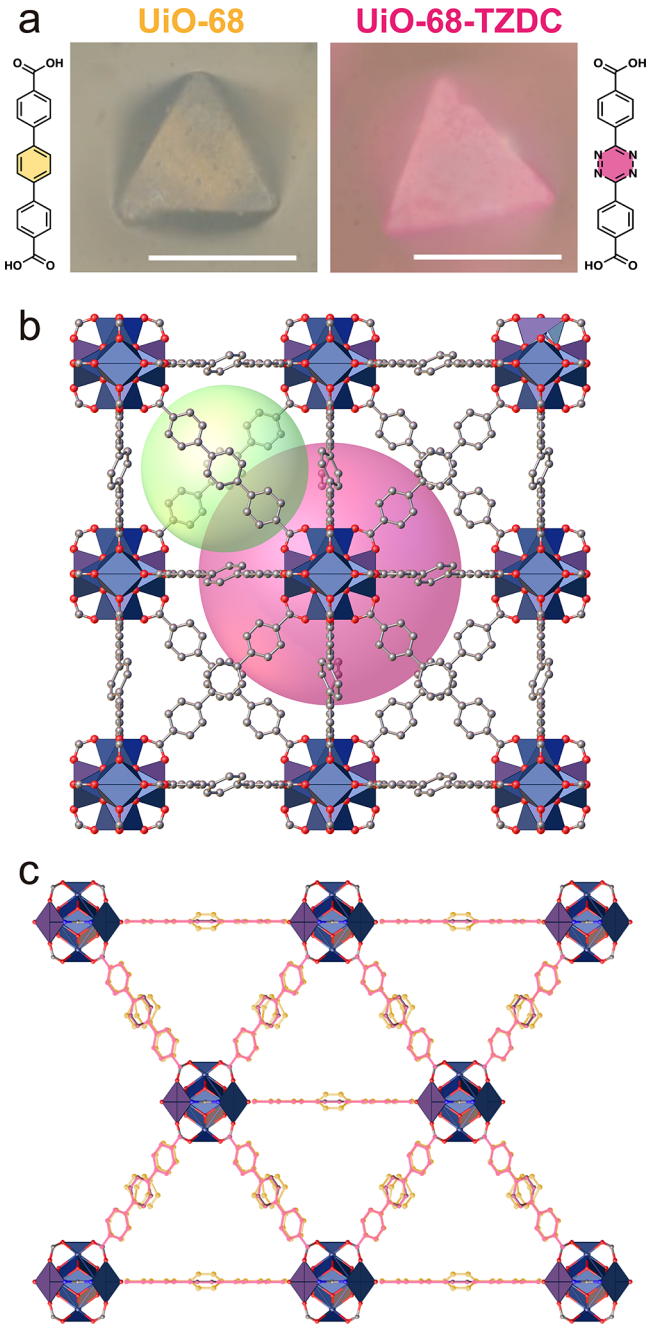

Figure 1. (a) (Left) size and morphology of UiO-68. Scale bars correspond to 50 μm. (Right) size and morphology of photoactive UiO-68-TZDC crystals. Scale bars correspond to 25 μm. (b) Structure of UiO-68 along the *c* axis showing the accessible volume corresponding to octahedral (pink sphere) and tetrahedral voids (green). (c) Overlay of the two crystallographic-distinct linker structures in (011) showing the slight differences that result from the replacement of TPDC with TZDC.

Porosity and Chemical Stability: Effect of the Linker. The effect of the tetrazine core is more notable in the thermal

https://dx.doi.org/10.1021/jacs.0c09015
J. Am. Chem. Soc. 2021, 143, 1798−1806

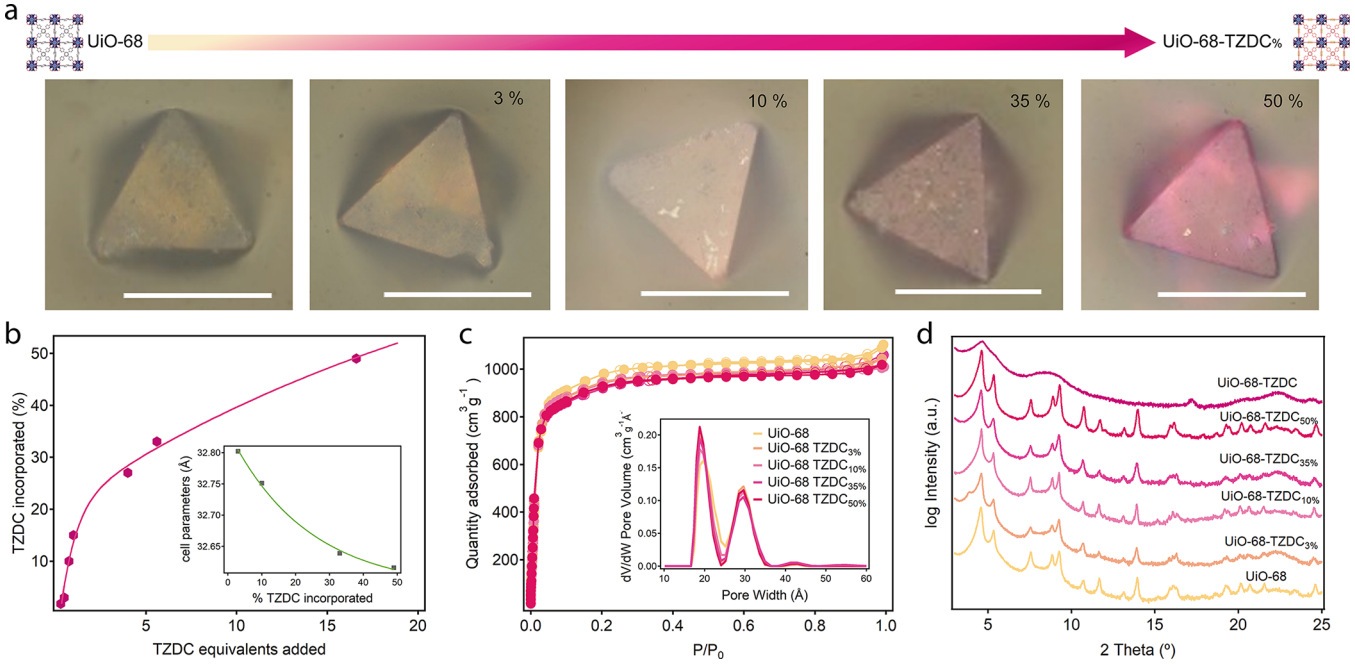

Figure 2. (a) Optical microscope images of UiO-68-TZDC$_{\%}$ samples. Scale bars correspond to 50 μm. (b) TZDC incorporated versus equivalents used in the synthesis. Inset: reduction of cell parameters as result of TZDC incorporation. (c) N_2 sorption isotherms at 77 K and PSD for UiO-68-TZDC$_{\%}$ samples. (Filled marker were used for adsorption and empty marker for desorption). (d) PXRD in logarithmic scale of intensity of the solids after soaked water: methanol (4:1, v/v%) for 24 h.

and chemical stability of the frameworks. Compared to UiO-68 that decomposes in air above 500 °C, the thermogravimetric analysis of UiO-68-TZDC shows a gradual decomposition from 250 to 450 °C indicative of the oxidation of the tetrazine core at high temperatures. The hydrolytic stability of the solids was evaluated by incubation in water for 24 h. The PXRDs after this treatment suggest that the structure of UiO-68 remains intact whereas UiO-68-TZDC undergoes partial amorphization (SI Section S4). The negative effect of TZDC on the strength of the framework linkages against hydrolysis is also confirmed by ICP studies, that show a superior leaching (22.4 $\mu g \cdot L^{-1}$) of zirconium to solution upon incubation of the solids in water/methanol mixtures (Figure S55). This agrees well with the weakening of the elongated coordination bonds in the last for feebler metal joints more prone to hydrolysis.

We next analyzed the effect of the linker in tuning the structural robustness of the solids for optimizing the process of activation, a critical step to access the expected surface areas.[19] We selected a range of solvents to examine the effect of changes in coordinating ability, polarity, or surface tension in the collapse of porosity (Table S5, Figures S15 and S17).[20] Methanol exchange leads to amorphization in both cases likely due to its ability to react with Zr_6 nodes.[21] In turn, acetone and DMF do not alter the structure of UiO-68 but provoke the collapse of UiO-68-TZDC. This suggests a negative effect of the electron-deficient heterocycle in maximizing the interaction with polar solvents for a framework more susceptible to the capillary-forces generated in the activation process. To confirm this point, we used hexane for minimizing the interaction with the framework due to its low surface tension (17.9 $mN \cdot m^{-1}$ at 25 °C) and small dipole moment (0.08 D). Exchange with hexane for 5 days, followed by drying in anhydrous conditions, for avoiding humidity and reducing capillary forces[22] is respectful with the structure of both materials. See SI Section S4.6 for more details. Both samples were degassed overnight at 60 °C and 10^{-6} Torr before gas analysis. They display a nonhysteretic, type-I N_2 adsorption isotherms with multipoint BET surface areas in excellent agreement with the expected values, 4028 and 4289 $m^2 \cdot g^{-1}$ for UiO-68 and UiO-68-TZDC, respectively.[1]

The Pore Size Distributions (PSDs) calculated by using Nonlinear Density Functional Theory (NLDFT) models reveal a narrow distribution of two types of mesopores centered at 2.0 and 3.0 nm, consistent with the pore size values calculated from the crystallographic data available (Table S6). Additional measurements collected for samples exchanged with wet hexane or methanol show a significant drop in surface area of 30% and 80% for UiO-68-TZDC, confirming the importance of minimizing solvent-framework interaction to access the expected porosity. Note that this is only critical for the activation step. After that, the solid can be exposed to open air with no impact over its surface area. CO_2 adsorption measurements reveal a modest uptake at 273 K of around 50 $cm^3 \cdot g^{-1}$. The calculated isosteric heats of adsorption confirm the positive effect of the nitrogenated core in UiO-68-TZDC for stronger interaction with the guest (Q_{st} = 31 $kJ \cdot mol^{-1}$). The properties of the single-linker phases reveal the necessity of combining both units in the same material to produce a photoactive material without compromising its chemical stability or porosity, both important to photocatalytic applications.

Multivariate Mesoporous Crystals by Solvent-Assisted Linker Exchange. We decided to investigate a HT library of reactions to produce multivariate MOFs[23] by direct combination of TPDC and TZDC with systematic control of ratio, temperature, concentration, and mixture of solvents. All attempts resulted in solids with reduced crystallinity and negligible incorporation of TZDC, suggesting important differences in the reactivity of the linkers with Zr(IV) (SI Section S5.1). On the basis of their structural similarity, we

https://dx.doi.org/10.1021/jacs.0c09015
J. Am. Chem. Soc. 2021, 143, 1798−1806

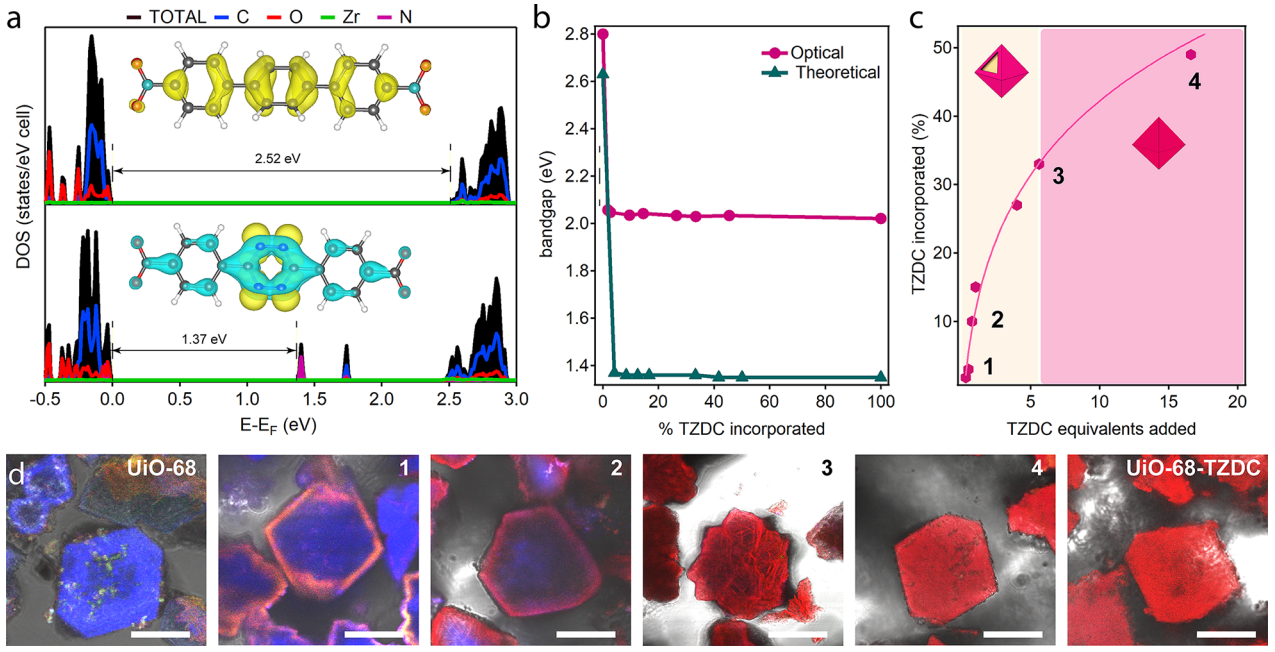

Figure 3. (a) Total (DOS, black) and projected (PDOS for each atoms) density of states for pristine UiO-68 (top) and UiO-68-TZDC$_{4\%}$, (bottom) calculated using PBE functional, this is a qualitative approach; the electronic structures could not be computed at the HSE06 level because of the system size. Inset: orbitals contributing to the HOCO (yellow) and LUCO (cyan) localized on the ligand. (b) Experimental and computed band gap values as a function of the TZDC incorporated. (c) Spatial linker arrangement in UiO-68-TZDC$_{\%}$ samples (pale yellow area for core−shell distribution and pink area for a more uniform distribution). (d) Fluorescence confocal microscope's images of polish UiO-68 samples reveal the resultant microstructures. Scale bars correspond to 25 and 10 μm for UiO-68 counterparts and UiO-68-TZDC, respectively.

decided to use postsynthetic linker exchange methods instead. By using UiO-68 crystals as precursors, we prepared a family of UiO-68-TZDC$_{\%}$ multivariate solids by SALE of varying equivalents of the tetrazine linker in DMF at 80 °C for 3 h. We used a base (Et_3N) to deprotonate H_2TZDC and favor the linker exchange (SI Section S5.2).[24] UiO-68-TZDC$_{\%}$ crystals were digested and analyzed by ^{1}H NMR (Nuclear Magnetic Resonance). The integration of the resonances for aromatic protons confirm the presence of both linkers and reveal a fine control over the exchange rate from 3 to 50%, concomitant with the color of the crystals (Figure 2a). The FT−IR spectra of the samples show a shift of 25 cm^{-1} in the $\upsilon_{C=O}$ vibration compared to the free linker. This rules out the trapping of TZDC in the mesopores of the MOF and confirms that the NMR quantification is representative of the actual incorporation of the linker to the framework. We used these techniques to analyze the maximum exchange ratio possible. Beyond UiO-68 TZDC$_{50\%}$, reactions with more than 20 equiv of TZDC show clear evidence of ineffective linker exchange in the final products. As shown in Figure 2b, UiO-68-TZDC$_{3-50\%}$ crystals show the same logarithmic rate of TZDC incorporation with the number of equivalents observed for other Zr-MOFs.[25] Phase purity was preliminary evaluated by PXRD Le Bail refinement of all solids. We observe a compression of the unit cell parameters that correlates well with the TZDC% incorporated. All solids display permanent porosity with negligible changes to their surface area and PSD compared to the single-linker phases (Figure 2c). SEM analysis rules out any morphological damage during linker exchange. All crystals retain the octahedral morphology and size of the UiO-68 seed, suggesting that the incorporation of TZDC operates in the crystal and does not involve their dissolution/recrystallization.

Besides respecting the structure and porosity of the pristine solids, the coexistence of TPDC and TZDC in multivariate UiO-68 crystals allows for reaching a fine balance between chemical stability and photoactivity. We soaked UiO-68-TZDC$_{3-50\%}$ crystals in water/methanol mixtures (4:1, v/v%) for 24 h. These methanolic solutions are often used to test the photocatalytic activity of MOFs in hydrogen evolution reactions.[11−13] Compared to UiO-68-TZDC that becomes amorphous, all solids retain their original structure with negligible changes in their PXRD patterns regardless the TZDC% incorporated (Figure 2d). Compared to minimum changes in structural stability, the impact of tetrazine doping on the hydrolytical stability of the multivariate frameworks is more acute. ICP analysis shows an increasing rate of metal leaching upon incorporation of TZDC. Linker sensitization is an efficient way to maximize the photocatalytic activity of MOFs with visible light by taking advantage of their synthetic/structural tunability. This strategy is dominated by porphyrins,[26] functionalized organic linkers,[27,28] or the incorporation of ruthenium or iridium complexes.[29] *s*-Tetrazine linkers are also excellent candidates in this regard due to the combination of one-electron reversible reduction behavior and visible-light sensitization.

Impact of Tetrazine Doping in the Electronic Structure of the Framework. To understand the effect of tetrazine doping, we calculated the electronic structure of the hybrid frameworks by using density functional theory (DFT, SI Section S6.1). Figure 3a shows a comparison of the electronic density of states diagram of pristine UiO-68 and UiO-68-TZDC$_{4\%}$, that corresponds to the incorporation of one TZDC linker per unit cell. In UiO-68, the position the highest occupied crystalline orbitals (HOCO) and the lowest unoccupied crystalline orbital (LUCO) is dominated by the aromatic 2p orbitals of TPDC. The introduction of a single TZDC linker per cell yields a LUCO that is also dominated by the linker but shows clear differences. The contribution of the

https://dx.doi.org/10.1021/jacs.0c09015
J. Am. Chem. Soc. 2021, 143, 1798−1806

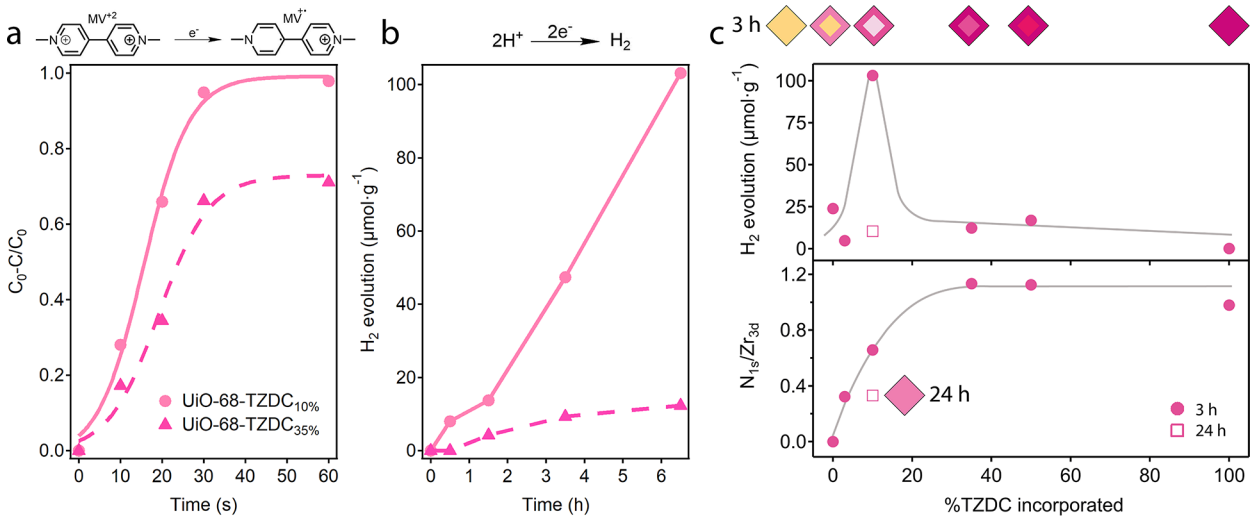

Figure 4. (a) Photocatalytic methyl viologen reduction yields after 1 min for UiO-68-TZDC$_{10\%}$ and UiO-68-TZDC$_{35\%}$. (b) Photocatalytic H_2 production after 6.5 h of irradiation for UiO-68-TZDC$_{10\%}$ (pink circles) and UiO-68-TZDC$_{35\%}$ (deep pink triangles). (c) (top) Accumulated H_2 production after 6.5 h of UiO-68, UiO-68-TZDC and multivariate UiO-68-TZDC$_x$ solids (x = 3, 10, 35, and 50%) prepared at 3 (filled circles) and 24 h (empty square). (bottom) XPS analysis of the changes in relative concentration of TZDC units in the surface of the crystals at a penetration depth of 10 nm. Solid lines are only a guide to the eye.

2p N and C orbitals from the tetrazine ring in UiO-68-TZDC$_{4\%}$ reduces the band gap to 1.37 eV compared to the 2.52 eV in UiO-68. We carried out additional calculations by systematically increasing the TZDC content up to 50% (12 linkers per unit cell). As shown in Figure 3a, the position of the LUCO is insensitive to increasing levels of doping and a single linker replacement is sufficient to dominate the electronic structure and optical properties of the hybrids. This effect is very similar to the modification of the band gap with monoaminated terephthalic linkers reported for MIL-125, that also saturates for the replacement of one linker per unit cell.[27]

To confirm the value of our computational simulations we used UV−vis solid reflectance measurements to estimate the optical band gap of UiO-68-TZDC$_{3-50\%}$ by using the Kubelka−Munk function. We observe an excellent match between the trend described by experimental results and computed band gap values, that further confirm the effectiveness of TZDC sensitization at very small doping levels (Figure 3b) (SI Section S6.2).

Chemical complexity in multivariate frameworks can be investigated with different techniques. Diffraction methods cannot account for linker or metal gradients across the crystal, but spectroscopic studies have been quite useful in solving this question. The spatial arrangement of organic crystals at different resolution can be elucidated with microscopic Attenuated Total Reflectance (ATR) infrared spectroscopy,[30] Solid-State Nuclear Magnetic Resonance (SS-NMR),[31] Photothermal Induced Resonance (PIR),[32] 2D Raman spectroscopy,[10] fluorescence confocal microscopy,[33] or fluorescence lifetime imaging.[34] Besides organic linkers, the spatial arrangement of multimetallic Secondary Building Units (SBUs) in multivariate frameworks has been also deciphered by using a combination of X-ray Photoelectron Spectroscopy (XPS) and UV−vis diffuse reflectance spectroscopy,[35] Scanning Transmission Electron Microscopy High-Angle Annular Dark Field imaging (STEM-HAADF),[36,37] or with atomic resolution by using atom probe tomography.[38] To analyze the spatial arrangement of parent and exchanged linkers in this case, we carried out fluorescence studies with a confocal microscope. Images were taken at different heights to account for the three-dimensional distribution of active TZDC and inactive TPDC linkers when excited with a green filter (λ = 559 nm). Comparison of UiO-68-TZDC at 3 and 35% doping levels suggests a higher concentration of TZCD linkers at the surface of the first based on more intense fluorescence at the edges and vertices of the crystal (SI Section S7 and Movies S1 and S2). For a clearer view of this phenomenon, we used an ultramicrotome to dissect and polish the section of the crystals. This experiment confirms that the crystals show an asymmetric distribution of linkers for the formation of core−shell/TPDC-TZDC architectures between 3 and 20% whereas this distribution becomes more uniform from 35% (Figure 3c,d). A closer analysis of the confocal images of the crystals after 3 and 10% doping also suggests that higher concentrations of TZDC seem to favor the formation of slightly thicker shells. To confirm if this asymmetric distribution of linkers was kinetically controlled, we also synthesized and characterized another set of UiO-68-TZDC$_{10\%}$ crystals by prolonging the exchange time to 6, 12, and 24 h while fixing the stochiometric equivalents of H_2TZDC in solution (SI Section S5.4). Compared to the core−shell distribution present after 3 h, reaction after 24 h seems to favor the diffusion of TZDC across the crystal for a more homogeneous distribution not distinguishable with confocal microscopy. XPS analysis of all samples confirms how longer reaction times induce and exponential decrease of the superficial concentration of TZDC, that seems to be kinetically controlled. Our data reveal how shorter reaction times are more likely to maximize the asymmetric distribution of linkers in multivariate frameworks prepared by linker-exchange reaction.

Overall, this confirms the ability of UiO-type materials to produce chemically diverse arrangements of functionalities after PSE as previously demonstrated with Raman and fluorescence imaging for UiO-66 and -67, respectively.[10,34] Our results point to a chemically diverse set of crystals with comparable optical band gaps ideal to investigate the effect of linker distribution over their photocatalytic activity. To the

https://dx.doi.org/10.1021/jacs.0c09015
J. Am. Chem. Soc. 2021, 143, 1798−1806

best of our knowledge, this still remains an open question for multivariate MOFs.

Interplay between Linker Distribution and Photocatalytic Activity. To investigate this possibility, we evaluated the photocatalytic performance of UiO-68, UiO-68-TZDC, and multivariate UiO-68-TZDC$_x$ solids (x = 3, 10, 35, and 50%) for the reduction of methyl viologen (MV) and the hydrogen evolution reaction (HER). As shown in Figure 4a, the different distribution of photoactive TZDC and inactive TPDC linkers promotes a much more efficient reduction of MV for UiO-68-TZDC$_{10\%}$ despite the reduced concentration of TZDC. This same trend is observed for the HER in a methanolic mixture (Figure 4b). Compared to the negligible activity of UiO-68-TZDC$_{35\%}$, UiO-68-TZDC$_{10\%}$ shows a linear increase in the H_2 production up to a maximum of ~100 μmol·g^{-1} after 6.5 h. This boost in performance is concomitant to an increase in the quantum efficiency of close to 15 times higher that might be associated with the formation of core−shell domains. It is worth commenting that related MOF-based photocatalysts, such as UiO-66, have shown negligible H_2 production in the absence of Pt nanoparticles or other cocatalysts, in good agreement with the production observed for UiO-68-TZDC$_{35\%}$.[39−41] We also observe a clear difference on the experimental BET value of both solids after the tests. Whereas UiO-68-TZDC$_{10\%}$ maintains a surface area close to the expected value, the 35% sample displays a clear reduction indicative of partial collapse of the structure or chemical damage (SI Section S8).

To investigate this effect in detail, we tested and compared the photocatalytic performance of UiO-68, UiO-68-TZDC, and multivariate UiO-68-TZDC$_x$ solids (x = 3, 10, 35, and 50%). As shown in Figure 4c, the accumulated H_2 production after 6.5 h increases with the TZCD% up to a maximum at 10% from which it goes sharply down to negligible values. This drastic change suggests that performance is somewhat controlled by the density of TZDC in the surface of the crystals. This was estimated for each case using XPS as the N/Zr ratio calculated from the integrated areas of the N_{1s} and Zr_{3d} survey spectra peaks. The XPS analysis reveals an increase in the nitrogen surface concentration consistent with the progressive replacement of parent TPDC by TZDC units for doping levels equal or below 10%, compared to the complete surface exchange that takes place from 35%. These results suggest a complex scenario in which performance is controlled not only by photoactive linker concentration but also by its distribution inside the crystal. On the basis of the analysis of pristine UiO-68-TZDC (vide supra), complete exchange might compromise the chemical and structural stability of the surface of the crystal at the conditions used in the photocatalytic tests. Compared to 35 and 50% for which complete surface exchange likely induces partial decomposition for an activity drop, the partial exchange at the surface of UiO-68-TZDC$_{10\%}$ is more suitable to reach a fine balance between photoactivity and stability. The stability of the frameworks was analyzed by ICP measurements of the solutions in conditions comparable to the photocatalytic tests. The rate of metal leaching remains below 10 μg·L^{-1} for doping levels below 35% but displays an increase from this point with the TZDC% in the crystal, suggesting reduced chemical stability for higher doping levels (SI Section S8). The poor H_2 production displayed by UiO-68-TZDC$_{10\%}$ prepared at 24 h also confirms the effect of TZDC surface concentration in the photocatalytic activity of this family of frameworks. Compared to the core−shell architecture formed after 3 h, the uniform distribution of photoactive linkers attained at longer reaction times is detrimental to overall performance.

CONCLUSIONS

Compared to the synthetic design of multiple component MOFs, which often relies only on the nature and relative percentage of the linkers combined as synthetic variables to tune the properties of the resulting materials, our results demonstrate also the impact of linker distribution as an efficient tool to code their function as previously demonstrated with porosity gradients.[42] These results confirm the importance of concentration and reaction time in controlling the relative ratio and distribution of mixed components in multivariate frameworks prepared by linker exchange reactions by using single crystals as a template. The reaction time seems to be particularly relevant in our case, as it seems to control linker diffusion to enable the formation of core−shell architectures under kinetic control. We are currently exploring this possibility to maximize the sensitization of multivariate titanium frameworks. Compared to Zr-MOFs for which photostimulated processes are mainly restricted to the linker,[43] Ti is more prone to induce ligand to metal charge transfer for higher photocatalytic efficiencies.[13,28]

EXPERIMENTAL SECTION

Synthesis of UiO-68. H_2TPDC (18 mg; 0.055 mmol) was suspended in a mixture of 3.5 mL of *N*,*N*-Dimethylformamide (DMF) and 150 μL of Trifluoroacetic Acid (TFA) (40 equiv) in a 5 mL Teflon vial. Subsequently, the $ZrCl_4$ (12 mg; 0.051 mmol) was added to the suspension. The bottle was sealed and heated in an oven at 100 °C for 72 h. After cooling down to room temperature, this results in the formation of deep yellow octahedral crystals that were isolated by centrifugation and washed with 45 mL of DMF (3 × 15 mL) and 45 mL of methanol (3 × 15 mL) in the centrifuge tube. The product was soaked in hexane for 3 days, after which it was dried at room temperature.

Synthesis of UiO-68-TZDC. H_2TZDC (18 mg; 0.055 mmol) was suspended in a mixture of 3.5 mL of DMF and 40 μL of TFA (10 equiv) in a 5 mL Teflon vial. Subsequently, the $ZrCl_4$ (12 mg; 0.051 mmol) was added to the suspension. The bottle was sealed and heated in an oven at 100 °C for 72 h. After cooling down to room temperature, this results in the formation of deep pink octahedral crystals that were isolated by centrifugation and washed with 45 mL of DMF (3 × 15 mL) and 45 mL of methanol (3 × 15 mL) in the centrifuge tube. The product was soaked in hexane for 7 days, after that it was dried at room temperature

Synthesis of Multivariate Solids. As-made UiO-68 (140 mg) was immersed in 54 mL of H_2TZDC solution in DMF and 40 μL of trimethylamine (Et_3N) at 80 °C under stirring. Using different equivalents of H_2TZDC (0−17 equiv) for 3 h of reaction produced a controllable UiO-68-TZDC$_{\%}$. After time reaction, the exchanged MOF was thoroughly washed with fresh DMF (40 mL × 5). The resultant solids were kept in hexane.

DFT Calculations. All structural calculation was performed using dispersion-corrected density functional theory (DFT-D3) with the Vienna Ab initio Simulation Package (VASP),[44,45] and employing the Perdew−Burke−Ernzerhof (PBE) functional.[46] The recommended GW PAW pseudopotentials[47] were used for all geometry and electronic calculations. A plane wave basis set was employed with a kinetic energy cutoff of 500 eV, and a Γ-point grid was used to sample the Brillouin zone. Electronic calculations was moreover performed with a 2 × 2 × 2 Γ-centered grid and PBE functional, although this functional is a qualitative approach, hybrid functional calculations on Zr-MOF have shown PBE to display the correct trends.[48,49] To investigate the effect of tetrazine doping has on the electronic structure, molecular substitutions were manually installed to the

https://dx.doi.org/10.1021/jacs.0c09015
J. Am. Chem. Soc. 2021, 143, 1798−1806

TPDC linker on experimentally determined unit cell of UiO-68, $[(Zr_6O_4(OH)_4)_4(TPDC)_{24}]$, and both lattice parameters and atomic positions were further relaxed.

Photocatalytic Methyl Viologen Reduction. Photoinduced electron transfer experiments were carried out using MOF dispersions (0.2 mg/mL) in water/methanol mixtures (4:1, v/v%) containing MV^{2+} (0.15 mM). The MOF dispersions containing MV^{2+} were sonicated, placed in a quartz cuvette capped with rubber septum and Ar purgued for 15 min prior irradiation with a 300 W Xe lamp. The UV−vis absorbance of the cuvettes was measured at different irradiation times. The photoinduced electron transfer measurements were followed by the decrease of the MV^{2+} absorption band centered at 260 nm as well as the increase of the $MV^{+\bullet}$ radical cation absorption bands at 395 and 605 nm.

Photocatalytic H_2 Production. A quartz photoreactor equipped with a manometer was loaded with sonicated dispersions of the corresponding MOFs at 1 mg/mL concentration in water/methanol (4:1, v/v) mixture. Prior irradiation the dispersions were purged with Ar for 15 min and pressurized at a final pressure of 1.3 bar. The photoreactor was located under the spot UV−vis light of an optic fiber from a 300 W Xe lamp at 110 mW/cm^2 for 6.5 h. The H_2 evolution was followed by injecting 250 μL of the reactor gases in an Agilent 490 MicroGC with a TC detector and Ar as carrier gas (MolSieve 5A column). Quantification of the percentage of each gas was based on prior calibration of the system injecting mixtures of H_2 and Ar with known percentage of gases. Quantum efficiency measurements were carried out measuring the lamp photon flux using a calibrated Si diode and taking into account the produced H_2.

■ ASSOCIATED CONTENT

Supporting Information

The Supporting Information is available free of charge at https://pubs.acs.org/doi/10.1021/jacs.0c09015.

Synthetic and experimental details; physical characterization and supporting tables and figures (PDF)

Movie S1, confocal images of UiO-68 TZDC3% showing the evolution of the fluorescence across the crystal (MP4)

Movies S2, confocal images of UiO-68 TZDC35% showing the evolution of the fluorescence across the crystal (MP4)

X-ray crystallographic data for UiO-68 (CIF)

X-ray crystallographic data for UiO-68-TZDC (CIF)

■ AUTHOR INFORMATION

Corresponding Authors

Carlos Martí-Gastaldo − *Functional Inorganic Materials Team, Instituto de Ciencia Molecular (ICMol), Universitat de València, 46980 València, Spain;* orcid.org/0000-0003-3203-0047; Email: carlos.marti@uv.es

Natalia M. Padial − *Functional Inorganic Materials Team, Instituto de Ciencia Molecular (ICMol), Universitat de València, 46980 València, Spain;* orcid.org/0000-0001-6067-3360; Email: nmpadial@ugr.es

Authors

Belén Lerma-Berlanga − *Functional Inorganic Materials Team, Instituto de Ciencia Molecular (ICMol), Universitat de València, 46980 València, Spain*

Carolina R. Ganivet − *Functional Inorganic Materials Team, Instituto de Ciencia Molecular (ICMol), Universitat de València, 46980 València, Spain*

Neyvis Almora-Barrios − *Functional Inorganic Materials Team, Instituto de Ciencia Molecular (ICMol), Universitat de València, 46980 València, Spain;* orcid.org/0000-0001-5269-2705

Sergio Tatay − *Functional Inorganic Materials Team, Instituto de Ciencia Molecular (ICMol), Universitat de València, 46980 València, Spain;* orcid.org/0000-0003-0785-866X

Yong Peng − *Instituto Universitario de Tecnología Química CSIC-UPV, Universitat Politècnica de València, 46022 València, Spain*

Josep Albero − *Instituto Universitario de Tecnología Química CSIC-UPV, Universitat Politècnica de València, 46022 València, Spain*

Oscar Fabelo − *Institut Laue Langevin, Grenoble, Cedex 9 38042, France;* orcid.org/0000-0001-6452-8830

Javier González-Platas − *Departamento de Física, Instituto Universitario de Estudios Avanzados en Física Atómica, Molecular y Fotónica (IUDEA), MALTA Consolider Team, Universidad de La Laguna, La Laguna, Tenerife E-38204, Spain;* orcid.org/0000-0003-3339-2998

Hermenegildo García − *Instituto Universitario de Tecnología Química CSIC-UPV, Universitat Politècnica de València, 46022 València, Spain;* orcid.org/0000-0002-9664-493X

Complete contact information is available at: https://pubs.acs.org/10.1021/jacs.0c09015

Notes

The authors declare no competing financial interest.

■ ACKNOWLEDGMENTS

This work was supported by the EU (ERC Stg Chem-fs-MOF 714122) and Spanish government (CTQ2017-83486-P, RTI2018-098568-A-I00, RYC-2016-1981, CEX2019-000919-M, PID2019-106383GB-C44/AEI/10.13039/501100011033 and RTI2018-098568-A-I00). B.L.-B. thanks the Spanish government for a FPU (FPU16/04162). S.T. thanks the Spanish government for a Ramón y Cajal Fellowship (RYC-2016-60719817). N.M.P. thanks the European Union for a Marie Skłodowska-Curie Global Fellowship (H2020-MSCA-IF-2016-GF-749359-EnanSET). J.G.P. thanks to the SIDIX at Servicios Generales de Apoyo a la Investigación (SEGAI) at La Laguna University. We also thank BSC-RES for computational resources (QS-2020-2-0024) and the University of Valencia for research facilities (Tirant and NANBIOSIS).

■ REFERENCES

(1) Cavka, J. H.; Jakobsen, S.; Olsbye, U.; Guillou, N.; Lamberti, C.; Bordiga, S.; Lillerud, K. P. A New Zirconium Inorganic Building Brick Forming Metal Organic Frameworks with Exceptional Stability. *J. Am. Chem. Soc.* **2008**, *130*, 13850−13851.

(2) Schaate, A.; Roy, P.; Godt, A.; Lippke, J.; Waltz, F.; Wiebcke, M.; Behrens, P. Modulated Synthesis of Zr-Based Metal-Organic Frameworks: From Nano to Single Crystals. *Chem. - Eur. J.* **2011**, *17*, 6643−6651.

(3) Furukawa, H.; Cordova, K. E.; O'Keeffe, M.; Yaghi, O. M. The Chemistry and Applications of Metal-Organic Frameworks. *Science* **2013**, *341*, 1230444.

(4) Yuan, S.; Feng, L.; Wang, K.; Pang, J.; Bosch, M.; Lollar, C.; Sun, Y.; Qin, J.; Yang, X.; Zhang, P.; Wang, Q.; Zou, L.; Zhang, Y.; Zhang, L.; Fang, Y.; Li, J.; Zhou, H.-C. Stable Metal−Organic Frameworks: Design, Synthesis, and Applications. *Adv. Mater.* **2018**, *30*, 1870277.

(5) Li, W.-Y.; Yang, S.; Li, Y.-A.; Li, Q.-Y.; Guan, Q.; Dong, Y.-B. Synthesis of an MOF-Based Hg^{2+}-Fluorescent Probe: Via Stepwise Post-Synthetic Modification in a Single-Crystal-to-Single-Crystal

Fashion and Its Application in Bioimaging. *Dalton Trans.* **2019**, *48*, 16502−16508.
(6) Tan, C.; Han, X.; Li, Z.; Liu, Y.; Cui, Y. Controlled Exchange of Achiral Linkers with Chiral Linkers in Zr-Based UiO-68 Metal-Organic Framework. *J. Am. Chem. Soc.* **2018**, *140*, 16229−16236.
(7) Gui, B.; Hu, G.; Zhou, T.; Wang, C. Pore Surface Engineering in a Zirconium Metal-Organic Framework via Thiol-Ene Reaction. *J. Solid State Chem.* **2015**, *223*, 79−83.
(8) Kim, M.; Cahill, J. F.; Fei, H.; Prather, K. A.; Cohen, S. M. Postsynthetic Ligand and Cation Exchange in Robust Metal-Organic Frameworks. *J. Am. Chem. Soc.* **2012**, *134*, 18082−18088.
(9) Karagiaridi, O.; Bury, W.; Sarjeant, A. A.; Stern, C. L.; Farha, O. K.; Hupp, J. T. Synthesis and Characterization of Isostructural Cadmium Zeolitic Imidazolate Frameworks via Solvent-Assisted Linker Exchange. *Chem. Sci.* **2012**, *3*, 3256−3260.
(10) Boissonnault, J. A.; Wong-Foy, A. G.; Matzger, A. J. Core-Shell Structures Arise Naturally during Ligand Exchange in Metal-Organic Frameworks. *J. Am. Chem. Soc.* **2017**, *139*, 14841−14844.
(11) Castells-Gil, J.; M. Padial, N.; Almora-Barrios, N.; Albero, J.; Ruiz-Salvador, A. R.; Gonzalez-Platas, J.; Garcia, H.; Marti-Gastaldo, C. Chemical Engineering of Photoactivity in Heterometallic Titanium-Organic Frameworks by Metal Doping. *Angew. Chem. Int. Ed.* **2018**, *130*, 8589−8593.
(12) Castells-Gil, J.; M. Padial, N.; Almora-Barrios, N.; da Silva, I.; Mateo, D.; Albero, J.; Garcia, H.; Marti-Gastaldo, C. De Novo Synthesis of Mesoporous Photoactive Titanium(IV)-Organic Frameworks with MIL-100 Topology. *Chem. Sci.* **2019**, *10*, 4313−4321.
(13) M. Padial, N.; Castells-Gil, J.; Almora-Barrios, N.; Romero-Angel, M.; da Silva, I.; Barawi, M.; Garcia-Sanchez, A.; de la Pena O'Shea, V. A.; Marti-Gastaldo, C. Hydroxamate Titanium-Organic Frameworks and the Effect of Siderophore-Type Linkers over Their Photocatalytic Activity. *J. Am. Chem. Soc.* **2019**, *141*, 13124−13133.
(14) Banerjee, R.; Phan, A.; Wang, B.; Knobler, C.; Furukawa, H.; O'Keeffe, M.; Yaghi, O. M. High-Throughput Synthesis of Zeolitic Imidazolate Frameworks and Application to CO2 Capture. *Science* **2008**, *319*, 939−943.
(15) Clavier, G.; Audebert, P. S -Tetrazines as Building Blocks for New Functional Molecules and Molecular Materials. *Chem. Rev.* **2010**, *110*, 3299−3314.
(16) Jang, H. S.; Jana, S.; Blizzard, R. J.; Meeuwsen, J. C.; Mehl, R. A. Access to Faster Eukaryotic Cell Labeling with Encoded Tetrazine Amino Acids. *J. Am. Chem. Soc.* **2020**, *142*, 7245−7249.
(17) Feng, L.; Lo, S.; Wang, S.; Tan, K.; Li, H.; Yuan, S.; Lin, Y.; Lin, C.; Wang, S.; Lu, K.; Zhou, H.-C. An Encapsulation-Rearrangement Strategy to Integrate Superhydrophobicity into Mesoporous Metal-Organic Frameworks. *Matter* **2020**, *2*, 988−999.
(18) Vinu, M.; Sivasankar, K.; Prabu, S.; Han, J.; Lin, C.; Yang, C.; Demel, J. Tetrazine-Based Metal-Organic Frameworks as Scaffolds for Post-Synthetic Modification by the Click Reaction. *Eur. J. Inorg. Chem.* **2020**, *5*, 461−466.
(19) Dodson, R. A.; Wong-Foy, A. G.; Matzger, A. J. The Metal−Organic Framework Collapse Continuum: Insights from Two-Dimensional Powder X-Ray Diffraction. *Chem. Mater.* **2018**, *30*, 6559−6565.
(20) Ayoub, G.; Islamoglu, T.; Goswami, S.; Friščić, T.; Farha, O. K. Torsion Angle Effect on the Activation of UiO Metal-Organic Frameworks. *ACS Appl. Mater. Interfaces* **2019**, *11*, 15788−15794.
(21) Yang, D.; Bernales, V.; Islamoglu, T.; Farha, O. K.; Hupp, J. T.; Cramer, C. J.; Gagliardi, L.; Gates, B. C. Tuning the Surface Chemistry of Metal Organic Framework Nodes: Proton Topology of the Metal-Oxide-Like Zr_6 Nodes of UiO-66 and NU-1000. *J. Am. Chem. Soc.* **2016**, *138*, 15189−15196.
(22) Mondloch, J. E.; Katz, M. J.; Planas, N.; Semrouni, D.; Gagliardi, L.; Hupp, J. T.; Farha, O. K. Are Zr_6-Based MOFs Water Stable? Linker Hydrolysis vs. Capillary-Force-Driven Channel Collapse. *Chem. Commun.* **2014**, *50*, 8944−8946.
(23) Deng, H.; Doonan, C. J.; Furukawa, H.; Ferreira, R. B.; Towne, J.; Knobler, C. B.; Wang, B.; Yaghi, O. M. Multiple Functional Groups of Varying Ratios in Metal-Organic Frameworks. *Science* **2010**, *327*, 846−850.
(24) Nickerl, G.; Senkovska, I.; Kaskel, S. Tetrazine Functionalized Zirconium MOF as an Optical Sensor for Oxidizing Gases. *Chem. Commun.* **2015**, *51*, 2280−2282.
(25) Marreiros, J.; Caratelli, C.; Hajek, J.; Krajnc, A.; Fleury, G.; Bueken, B.; De Vos, D. E.; Mali, G.; Roeffaers, M. B. J.; Van Speybroeck, V.; Ameloot, R. Active Role of Methanol in Post-Synthetic Linker Exchange in the Metal-Organic Framework UiO-66. *Chem. Mater.* **2019**, *31*, 1359−1369.
(26) Fateeva, A.; Chater, P. A.; Ireland, C. P.; Tahir, A. A.; Khimyak, Y. Z.; Wiper, P. V.; Darwent, J. R.; Rosseinsky, M. J. A Water-Stable Porphyrin-Based Metal-Organic Framework Active for Visible-Light Photocatalysis. *Angew. Chem. Int. Ed.* **2012**, *51*, 7440−7444.
(27) Hendon, C. H.; Tiana, D.; Fontecave, M.; Sanchez, C.; D'Arras, L.; Sassoye, C.; Rozes, L.; Mellot-Draznieks, C.; Walsh, A. Engineering the Optical Response of the Titanium-MIL-125 Metal-Organic Framework through Ligand Functionalization. *J. Am. Chem. Soc.* **2013**, *135*, 10942−10945.
(28) Chambers, M. B.; Wang, X.; Ellezam, L.; Ersen, O.; Fontecave, M.; Sanchez, C.; Rozes, L.; Mellot-Draznieks, C. Maximizing the Photocatalytic Activity of Metal-Organic Frameworks with Aminated-Functionalized Linkers: Substoichiometric Effects in MIL-125-NH_2. *J. Am. Chem. Soc.* **2017**, *139*, 8222−8228.
(29) Elcheikh Mahmoud, M.; Audi, H.; Assoud, A.; Ghaddar, T. H.; Hmadeh, M. Metal-Organic Framework Photocatalyst Incorporating Bis(4′-(4-Carboxyphenyl)-Terpyridine)Ruthenium(II) for Visible-Light-Driven Carbon Dioxide Reduction. *J. Am. Chem. Soc.* **2019**, *141*, 7115−7121.
(30) Furukawa, S.; Hirai, K.; Takashima, Y.; Nakagawa, K.; Kondo, M.; Tsuruoka, T.; Sakata, O.; Kitagawa, S. A Block PCP Crystal: Anisotropic Hybridization of Porous Coordination Polymers by Face-Selective Epitaxial Growth. *Chem. Commun.* **2009**, 5097−5099.
(31) Kong, X.; Deng, H.; Yan, F.; Kim, J.; Swisher, J. A.; Smit, B.; Yaghi, O. M.; Reimer, J. A. Mapping of Functional Groups in Metal-Organic Frameworks. *Science* **2013**, *341*, 882−885.
(32) Katzenmeyer, A. M.; Canivet, J.; Holland, G.; Farrusseng, D.; Centrone, A. Assessing Chemical Heterogeneity at the Nanoscale in Mixed-Ligand Metal−Organic Frameworks with the PTIR Technique. *Angew. Chem. Int. Ed.* **2014**, *53*, 2852−2856.
(33) Jayachandrababu, K. C.; Sholl, D. S.; Nair, S. Structural and Mechanistic Differences in Mixed-Linker Zeolitic Imidazolate Framework Synthesis by Solvent Assisted Linker Exchange and de Novo Routes. *J. Am. Chem. Soc.* **2017**, *139*, 5906−5915.
(34) Schrimpf, W.; Jiang, J.; Ji, Z.; Hirschle, P.; Lamb, D. C.; Yaghi, O. M.; Wuttke, S. Chemical Diversity in a Metal-Organic Framework Revealed by Fluorescence Lifetime Imaging. *Nat. Commun.* **2018**, *9*, 1647.
(35) Liu, Q.; Cong, H.; Deng, H. Deciphering the Spatial Arrangement of Metals and Correlation to Reactivity in Multivariate Metal−Organic Frameworks. *J. Am. Chem. Soc.* **2016**, *138*, 13822−13825.
(36) Luo, T.-Y.; Liu, C.; Gan, X. Y.; Muldoon, P. F.; Diemler, N. A.; Millstone, J. E.; Rosi, N. L. Multivariate Stratified Metal−Organic Frameworks: Diversification Using Domain Building Blocks. *J. Am. Chem. Soc.* **2019**, *141*, 2161−2168.
(37) M. Padial, N.; Lerma-Berlanga, B.; Almora-Barrios, N.; Castells-Gil, J.; da Silva, I.; de la Mata, M.; Molina, S. I.; Hernandez-Saz, J.; Platero-Prats, A. E.; Tatay, S.; Mart-Gastaldo, C. Heterometallic Titanium−Organic Frameworks by Metal-Induced Dynamic Topological Transformations. *J. Am. Chem. Soc.* **2020**, *142*, 6638−6648.
(38) Ji, Z.; Li, T.; Yaghi, O. M. Sequencing of Metals in Multivariate Metal-Organic Frameworks. *Science* **2020**, *369* (6504), 674−680.
(39) Gomes Silva, C.; Luz, I.; Llabres i Xamena, F. X.; Corma, A.; Garcia, H. Water Stable Zr-Benzenedicarboxylate Metal-Organic Frameworks as Photocatalysts for Hydrogen Generation. *Chem. - Eur. J.* **2010**, *16*, 11133−11138.
(40) Lin, R.; Shen, L.; Ren, Z.; Wu, W.; Tan, Y.; Fu, H.; Zhang, J.; Wu, L. Enhanced Photocatalytic Hydrogen Production Activity via

https://dx.doi.org/10.1021/jacs.0c09015
J. Am. Chem. Soc. 2021, 143, 1798−1806

Dual Modification of MOF and Reduced Graphene Oxide on CdS. *Chem. Commun.* **2014**, *50*, 8533−8535.
(41) Wang, R.; Gu, L.; Zhou, J.; Liu, X.; Teng, F.; Li, C.; Shen, Y.; Yuan, Y. Quasi-Polymeric Metal-Organic Framework UiO-66/g-C_3N_4 Heterojunctions for Enhanced Photocatalytic Hydrogen Evolution under Visible Light Irradiation. *Adv. Mater. Interfaces* **2015**, *2*, 1500037.
(42) Liu, C.; Zeng, C.; Luo, T.-Y.; Merg, A. D.; Jin, R.; Rosi, N. L. Establishing Porosity Gradients within Metal−Organic Frameworks Using Partial Postsynthetic Ligand Exchange. *J. Am. Chem. Soc.* **2016**, *138*, 12045−12048.
(43) Nasalevich, M. A.; Hendon, C. H.; Santaclara, J. G.; Svane, K.; van der Linden, B.; Veber, S. L.; Fedin, M. V.; Houtepen, A. J.; van der Veen, M. A.; Kapteijn, F.; Walsh, A.; Gascon, J. Electronic Origins of Photocatalytic Activity in d0Metal Organic Frameworks. *Sci. Rep.* **2016**, *6*, 23676.
(44) Kresse, G.; Furthmüller, J. Efficiency of Ab-Initio Total Energy Calculations for Metals and Semiconductors Using a Plane-Wave Basis Set. *Comput. Mater. Sci.* **1996**, *6*, 15−50.
(45) Kresse, G.; Furthmüller, J. Efficient Iterative Schemes for Ab Initio Total-Energy Calculations Using a Plane-Wave Basis Set. *Phys. Rev. B: Condens. Matter Mater. Phys.* **1996**, *54*, 11169−11186.
(46) Perdew, J. P.; Burke, K.; Ernzerhof, M. Generalized Gradient Approximation Made Simple. *Phys. Rev. Lett.* **1996**, *77*, 3865−3868.
(47) Lejaeghere, K.; Bihlmayer, G.; Björkman, T.; Blaha, P.; Blügel, S.; Blum, V.; Caliste, D.; Castelli, I. E.; Clark, S. J.; Dal Corso, A.; de Gironcoli, S.; Deutsch, T.; Dewhurst, J. K.; Di Marco, I.; Draxl, C.; Dułak, M.; Eriksson, O.; Flores-Livas, J. A.; Garrity, K. F.; Genovese, L.; Giannozzi, P.; Giantomassi, M.; Goedecker, S.; Gonze, X.; Grånäs, O.; Gross, E. K.; Gulans, A.; Gygi, F.; Hamann, D. R.; Hasnip, P. J.; Holzwarth, N. A.; Iuşan, D.; Jochym, D. B.; Jollet, F.; Jones, D.; Kresse, G.; Koepernik, K.; Küçükbenli, E.; Kvashnin, Y. O.; Locht, I. L.; Lubeck, S.; Marsman, M.; Marzari, N.; Nitzsche, U.; Nordström, L.; Ozaki, T.; Paulatto, L.; Pickard, C. J.; Poelmans, W.; Probert, M. I.; Refson, K.; Richter, M.; Rignanese, G. M.; Saha, S.; Scheffler, M.; Schlipf, M.; Schwarz, K.; Sharma, S.; Tavazza, F.; Thunström, P.; Tkatchenko, A.; Torrent, M.; Vanderbilt, D.; van Setten, M. J.; Van Speybroeck, V.; Wills, J. M.; Yates, J. R.; Zhang, G. X.; Cottenier, S. Reproducibility in density functional theory calculations of solids. *Science* **2016**, *351*, 1415.
(48) De Vos, A.; Hendrickx, K.; Van Der Voort, P.; Van Speybroeck, V.; Lejaeghere, K. Missing Linkers: An Alternative Pathway to UiO-66 Electronic Structure Engineering. *Chem. Mater.* **2017**, *29*, 3006−3019.
(49) Hendrickx, K.; Vanpoucke, D. E. P.; Leus, K.; Lejaeghere, K.; Van Yperen-De Deyne, A.; Van Speybroeck, V.; Van Der Voort, P.; Hemelsoet, K. Understanding Intrinsic Light Absorption Properties of UiO-66 Frameworks: A Combined Theoretical and Experimental Study. *Inorg. Chem.* **2015**, *54*, 10701−10710.

https://dx.doi.org/10.1021/jacs.0c09015
J. Am. Chem. Soc. 2021, 143, 1798−1806